Electronic Supplementary Material (ESI) for Green Chemistry.
This journal is © The Royal Society of Chemistry 2020

Cellulose Nanocrystals (CNCs) as Hard Templates for Preparing Mesoporous Zeolite Y Assemblies with High Catalytic Activity

Electronic Supporting Information (ESI)

Oxidation of CNTs

TEM analysis of the pristine CNTs is shown in Fig. S1a. CNTs have outer diameters of approximately 10 nm. CNTs are intrinsically hydrophobic, consequently, it may be difficult to disperse CNTs during the preparation of seed-CNTs composites, resulting in the phase separation complication between the CNTs and zeolite during crystallisation. The CNTs tend to aggregate with their peers on the surface of neighbouring CNTs in aqueous solutions, causing significant phase separation problems between zeolite seed gel and carbon nanotubes during zeolite crystallisation. Accordingly, before use, CNTs were treated using NaOCl to make their surface hydrophilic. In a typical procedure, 200 mg CNTs was added to 100 mL of NaOCl solution, and stirred at room temperature for 24 h, followed by filtration, washing (with deionised water) and drying at 110 °C overnight. Comparative TEM analysis of the pristine and oxidised CNTs are shown in Fig. S1, showing that the oxidation treatment did not significantly affect the outer diameter of CNTs.

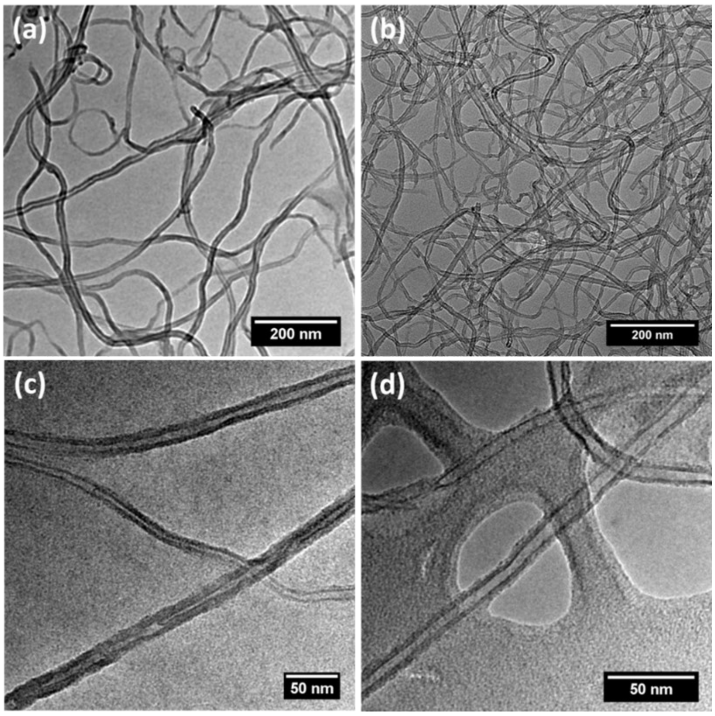

Fig. S1.TEM micrographs of (a,c) pristine CNTs and (b,d) oxidised CNTs.

Comparative FT-IR analysis of the pristine and oxidised CNTs was performed, as shown in Fig. S2, in comparison with the pristine CNTs, the spectrum of the oxidised CNTs presents additional bands. The bands at around 2,532–2,970 cm^{-1} can be attributed to stretching bands from the -COOH and -COH groups and -OH stretching from the strongly H-bonded-COOH, respectively. The bands at around 1,665 cm^{-1} can be assigned to the stretching variations of C=O group whereas the peak at around 1,411 cm^{-1} is associated to the carboxylate anion stretching mode. The band at about 1,036–1,281 cm^{-1} is related to C-O stretching of alcoholic compounds which approves that the carboxylic groups (-COOH) form on the surface of the oxidized CNTs by NaOCl.[1, 2] It is clear that these functional groups are present at the external and internal surface of oxidised CNTs, which may potentially help to increase the surface polarity and hence the compatibility during the synthesis of CNTs-Y zeolites. Addtionally, FT-IR analysis of CNCs (Fig. S2) shows that the presence of many surface groups. Bands located at 3,323, 2,900, 1,432 and 1,369 cm^{-1} correspond to the stretching modes of C-H. The band at 1,057 cm^{-1} can be attributed to C-O stretching, while the one at 1,652 cm^{-1} is ascribed to the -OH bond. The peak at 900 cm^{-1} shows the rocking vibration of -C-H band in CNCs.[3, 4]

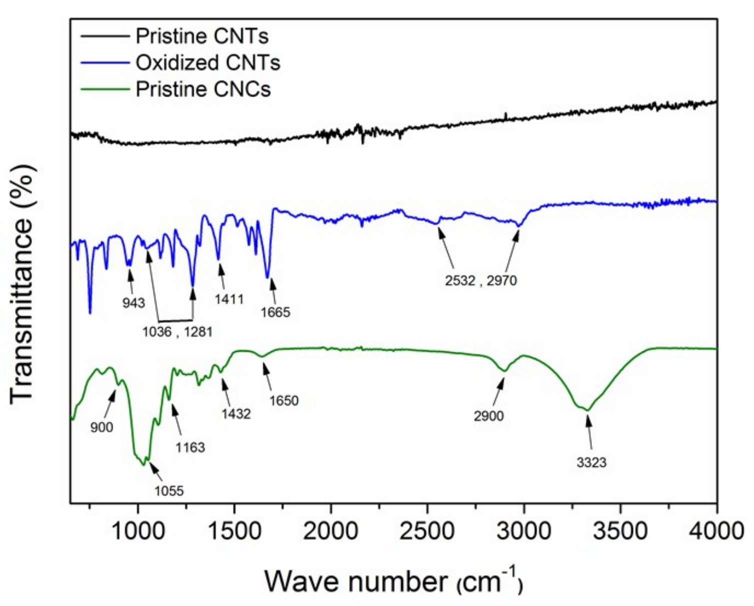

Fig S2. FT-IR spectra of the pristine and oxidised CNTs, and pristine CNCs.

GC Method and Calibration

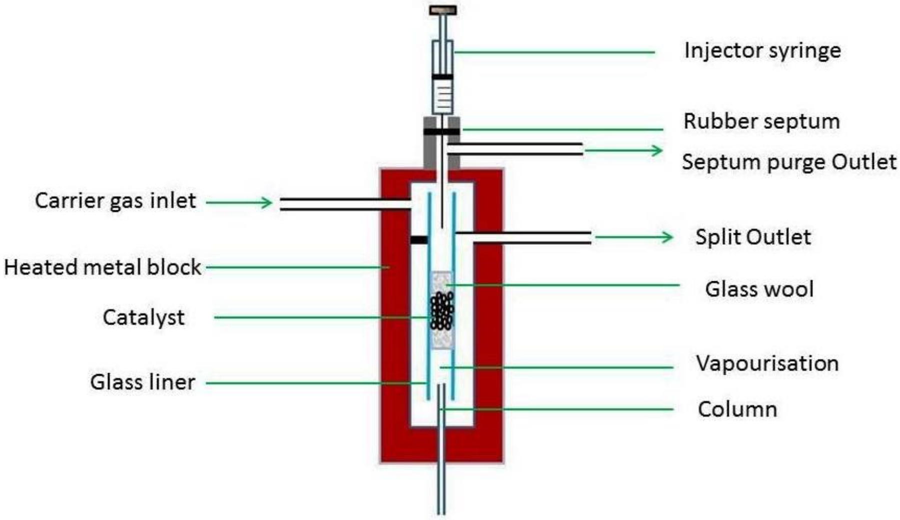

Fig. S3. Schematic diagram of the GC reactor for the pulse method used for the catalytic cracking of TiPBz.

Table S1. GC method used in this work.

Injection	- Injection volume = 0.2 µl (manual injection)
Inlets	- Heater temperature = 325 °C - Split ratio = 200:1 - Pressure = 16 psig - Flow rate = 200 mL min^{-1}
Column & Oven	- Stabilwax® (0.32 mm i.d., 30 m length, 1 µm film thickness) - Carrier gas = He (at 200 mL min^{-1}) Temperature programme: - Initial temperature = 80 °C (Oven) - Initial hold time at 80°C = 5 min - Heating rate = 10 °C min^{-1} - Final temperature = 220 °C - Final hold time at 220 °C = 10 min
Detector	- Detector type = Flame ionization detector (FID) - Detector temperature = 300 °C

GC was calibrated to establish a GC method and identify the retention times (RT) of reactants/products for the reaction analysis (using the area normalisation method). Calibration was performed by injecting equal amounts of the cracking products into the GC to allow the creation of a suitable method (Table S1) for peak separation and component analysis. GC calibration chromatographs were shown in Fig. S4. The analysis time for each injection was approximately 30 min. The total time of 17 injections were about 9 hours.

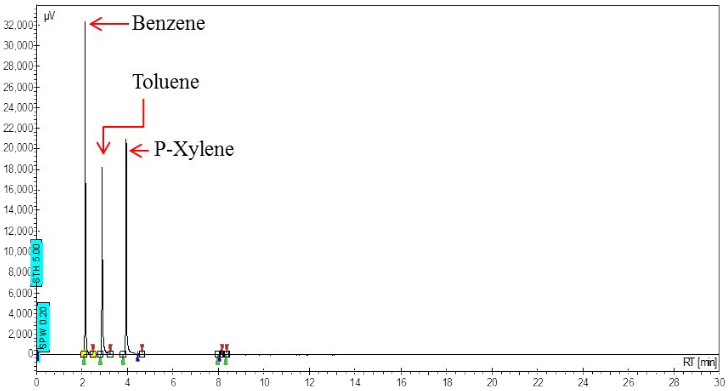
µV
Benzene
Toluene
P-Xylene
STH 5.00
SPW 0.20
32,000
30,000
28,000
26,000
24,000
22,000
20,000
18,000
16,000
14,000
12,000
10,000
8,000
6,000
4,000
2,000
0
RT [min]
0
2
4
6
8
10
12
14
16
18
20
22
24
26
28
30

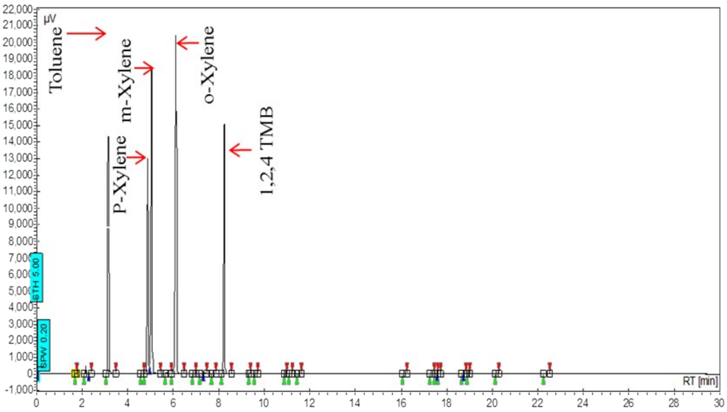
µV
Toluene
P-Xylene
m-Xylene
o-Xylene
1,2,4 TMB
STH 5.00
SPW 0.20
22,000
21,000
20,000
19,000
18,000
17,000
16,000
15,000
14,000
13,000
12,000
11,000
10,000
9,000
8,000
7,000
6,000
5,000
4,000
3,000
2,000
1,000
0
-1,000
RT [min]
0
2
4
6
8
10
12
14
16
18
20
22
24
26
28
30

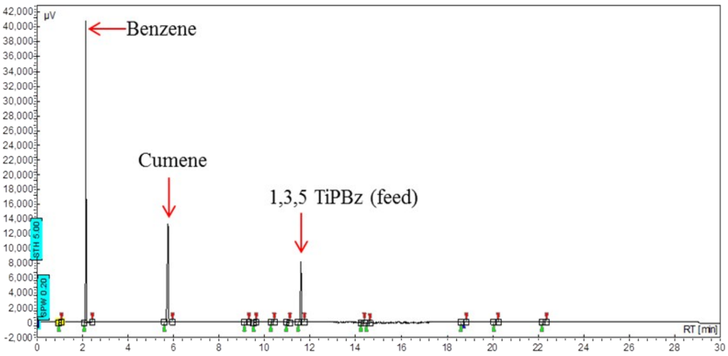
µV
Benzene
Cumene
1,3,5 TiPBz (feed)
STH 5.00
SPW 0.20
42,000
40,000
38,000
36,000
34,000
32,000
30,000
28,000
26,000
24,000
22,000
20,000
18,000
16,000
14,000
12,000
10,000
8,000
6,000
4,000
2,000
0
-2,000
RT [min]
0
2
4
6
8
10
12
14
16
18
20
22
24
26
28
30

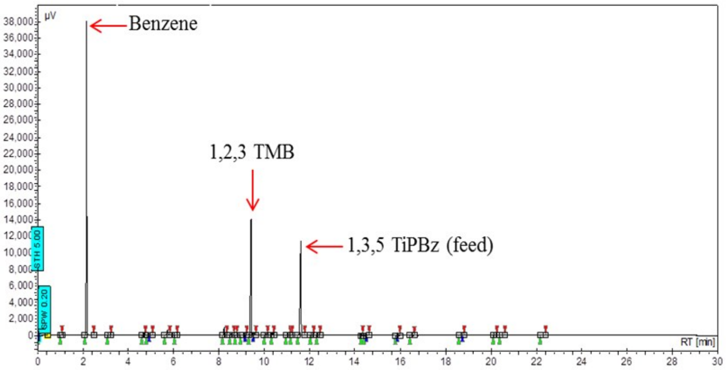
µV
Benzene
1,2,3 TMB
1,3,5 TiPBz (feed)
STH 5.00
SPW 0.20
38,000
36,000
34,000
32,000
30,000
28,000
26,000
24,000
22,000
20,000
18,000
16,000
14,000
12,000
10,000
8,000
6,000
4,000
2,000
0
RT [min]
0
2
4
6
8
10
12
14
16
18
20
22
24
26
28
30

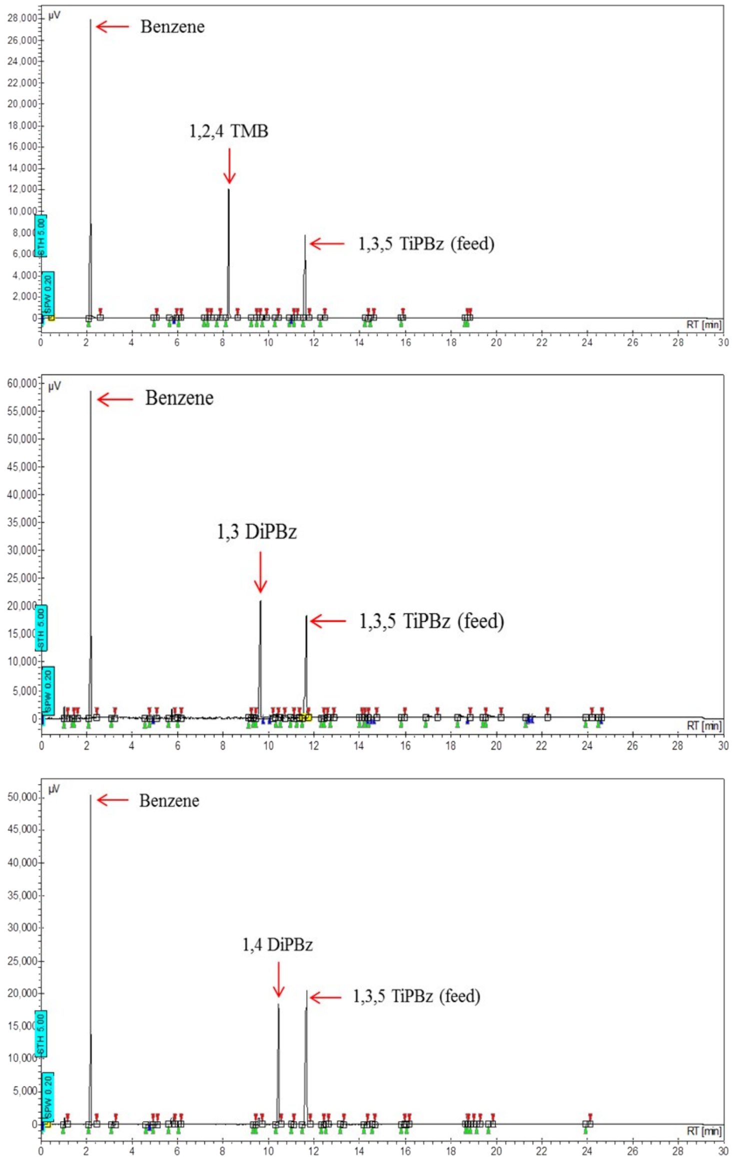

Fig. S4. GC calibration chromatographs.

Systematic Study of Secondary Growth Synthesis of zeolite Y

A systematic study of the secondary growth synthesis of zeolite Y was performed by varying the crystallisation time from 6 to 72 h (with the 6 h increments) at 100 °C while the seed ageing time was fixed at 24 h at RT. With reference to the simulated XRD pattern of zeolite Y as (Fig. S5a), it was noticed that zeolite Y phase did not start to appear until the crystallisation time of 12 h had passed due to the incomplete crystallisation of the amorphous feedstock around the seeds. XRD patterns of the synthesised NaY zeolites with different crystallisation times of 18 to 48 h showed the evident characteristic diffraction peaks of zeolite Y crystalline phase (i.e. at 2 theta (θ) of 6, 10, 12, 16, 19, 21, 23, 24, 27,30, 31, 32 and 34°), indicating the successful synthesis of Y zeolite. Based on XRD analysis, we found that the crystallisation time between 30 to 48 h was necessary to produce zeolite Y.

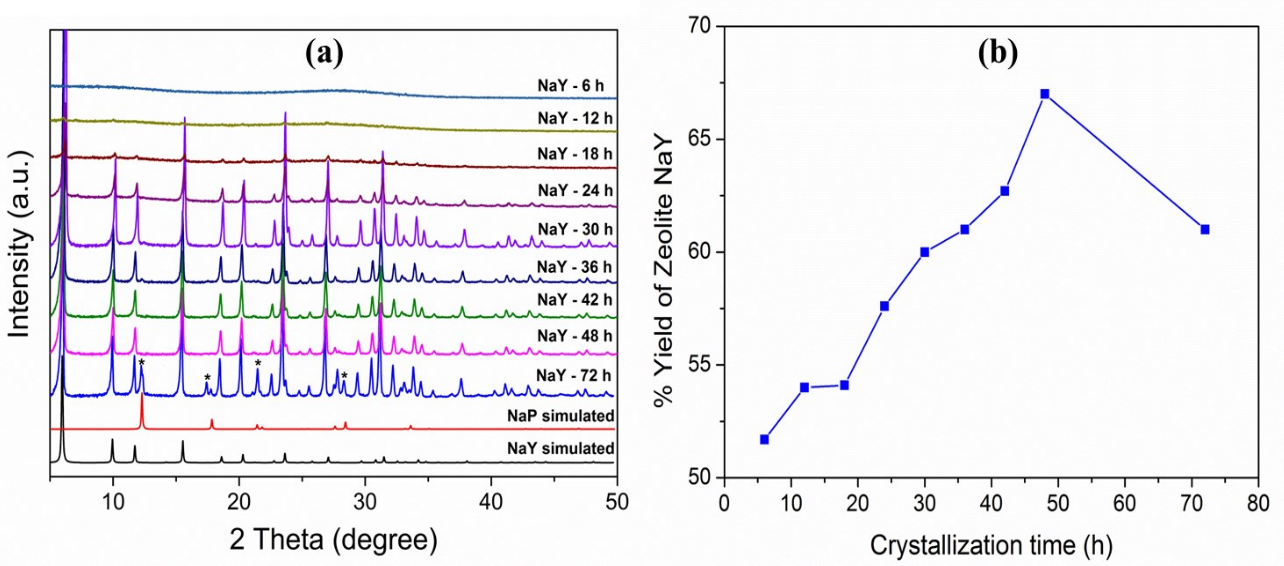

Fig. S5. (a) XRD patterns and (b) %yield of the as-prepared samples with different crystallisation time.

The yield of Y zeolites (defined by Eq. S1) is presented in Fig. S5b, showing that the yield of Y zeolite increased gradually from about 53 % at crystallisation time of 18 h to about 67 % at a crystallisation time of 48 h, then dropped to ca. 61% at 72 h. By extending the synthesis time to 72 h, the Y phase was likely to be dissolved and further transformed into another phase, as suggested by the additional XRD peaks (marked by star sign) in the 72 h sample in Fig. S5a.

$$\%\text{Yield} = \frac{\text{Actual yield}}{\text{Theoretical yield}} \times 100 \qquad \text{S1}$$

where the actual yield is the dry mass of the as-made Y zeolites, and the theoretical yield is the calculated mass (4 g) based on the limiting reactant used in the preparation recipe.

The additional peaks in the 72 h sample are characteristic peaks of zeolite P-GIS (a part of Gismondine group).[5-7] This observation is in a good agreement with the previous work contacted by the Supattra et. al., in which a crystallisation time >72 h was found to lead to the transformation of zeolite Y into P.[5-7] Therefore, based on the findings of this study, an optimum crystallisation time for the synthesis of NaY zeolite was established at 48 h.

The transformation of Y zeolite from the secondary growth synthesis was also evidenced by SEM analysis. Figs. S6a–S6c show the morphology of samples with synthesis times of 6, 12 and 18 h, respectively, suggesting the major presence of amorphous phase, rather than the crystallised phase, in these samples. With an increase of the crystallisation time to 24 h, it was revealed that the sample crystallised gradually, forming large crystals (Fig. S6d). By extending the crystallisation time further to 30, 36, 42 and 48 h (Figs. S6e–S6h), the typical octahedral morphology of Y zeolite exhibited with smooth surfaces, sharp edges and crystal sizes of ca. 2.5 µm. However, at a crystallisation time of 72 h, SEM analysis (Fig. S4i) shows the morphology of dissolved crystals with sphere-like shapes and less sharp edges, similar to zeolite P, confirming the formation of zeolite P.

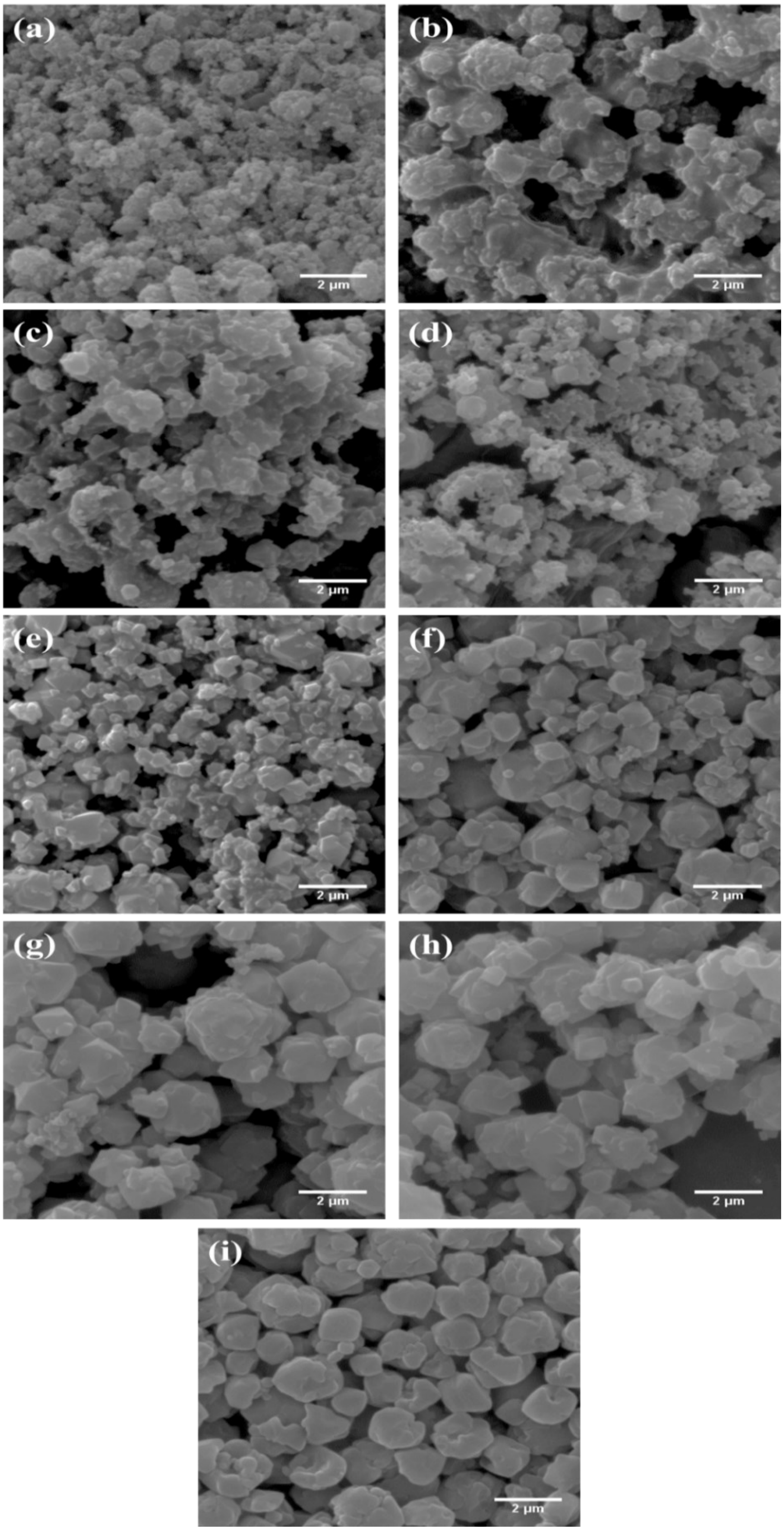

Fig. S6. SEM micrographs of samples obtained by the secondary growth synthesis at different crystallisation time of (a) 6 h, (b) 12 h, (c) 18 h, (d) 24 h, (e) 30 h, (f) 36 h, (g) 42 h, (h) 48 h, (i) 72 h.

Additional Characterisation of CNTs-Y and CNCs-Y

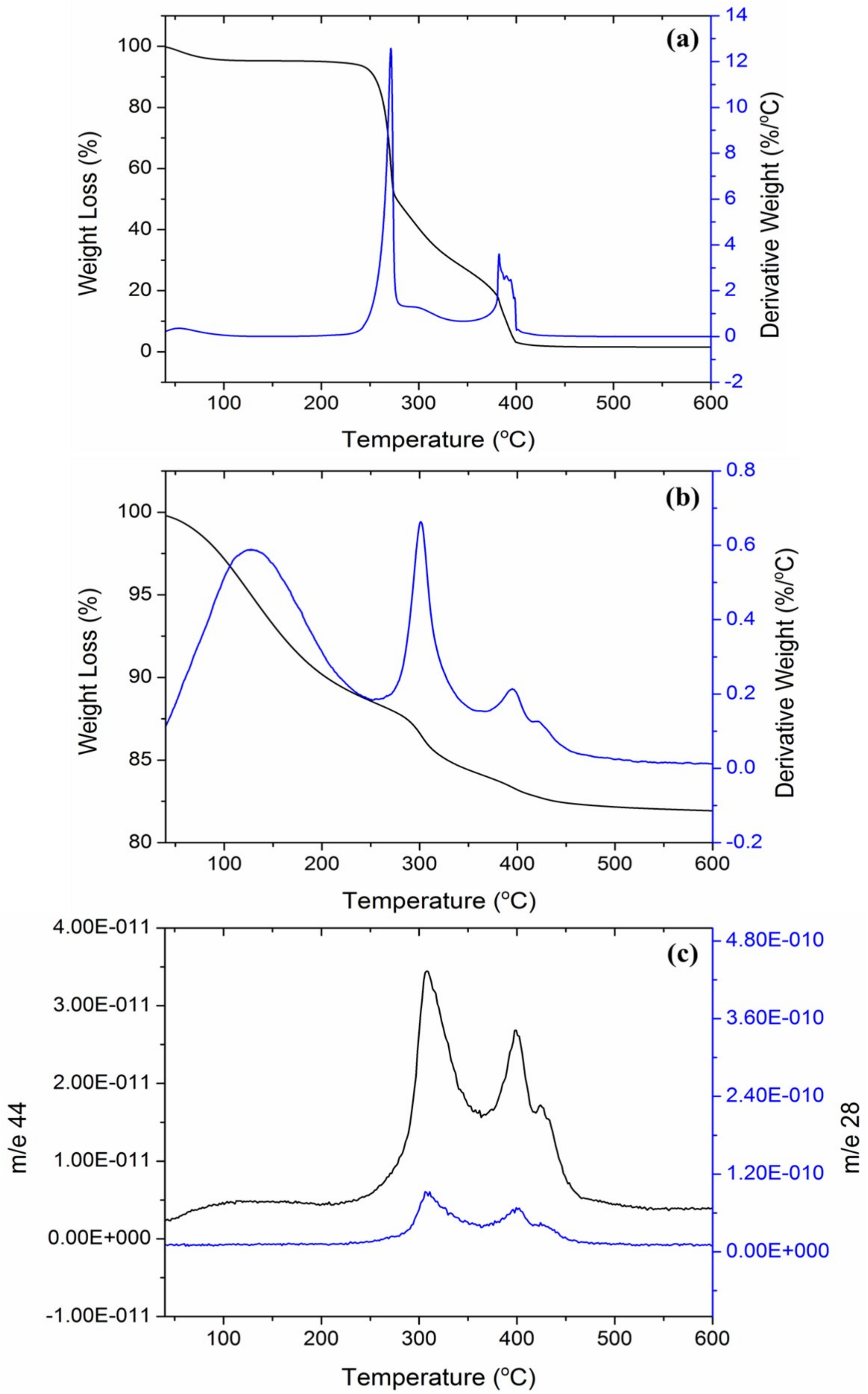

Fig. S7. (a) TGA of CNCs, (b) CNCs-Y and (c) MS analysis of CNCs-Y TGA.

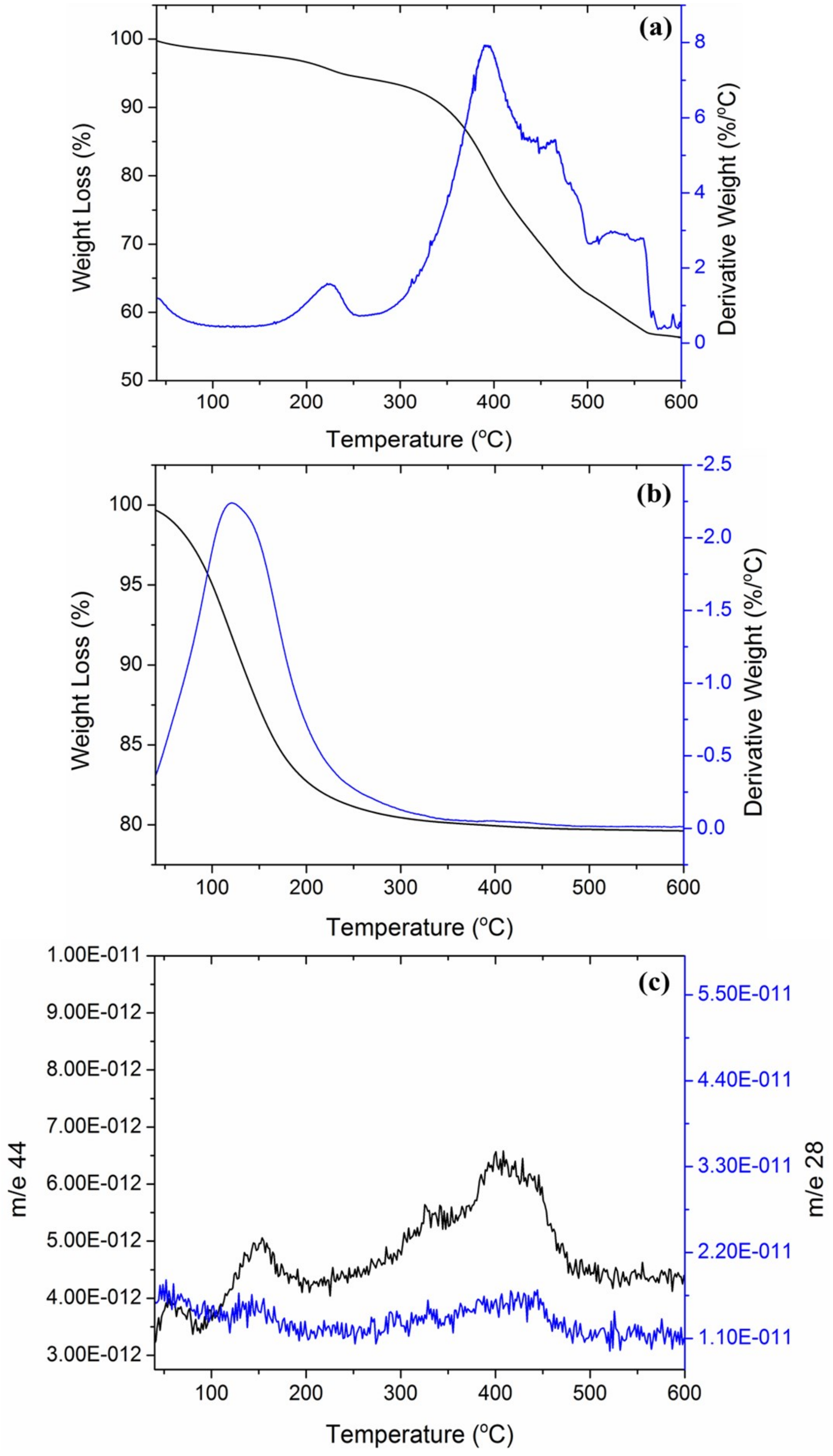

Fig. S8. (a) TGA of CNTs, (b) CNTs-Y and (c) MS analysis of CNTs-Y TGA.

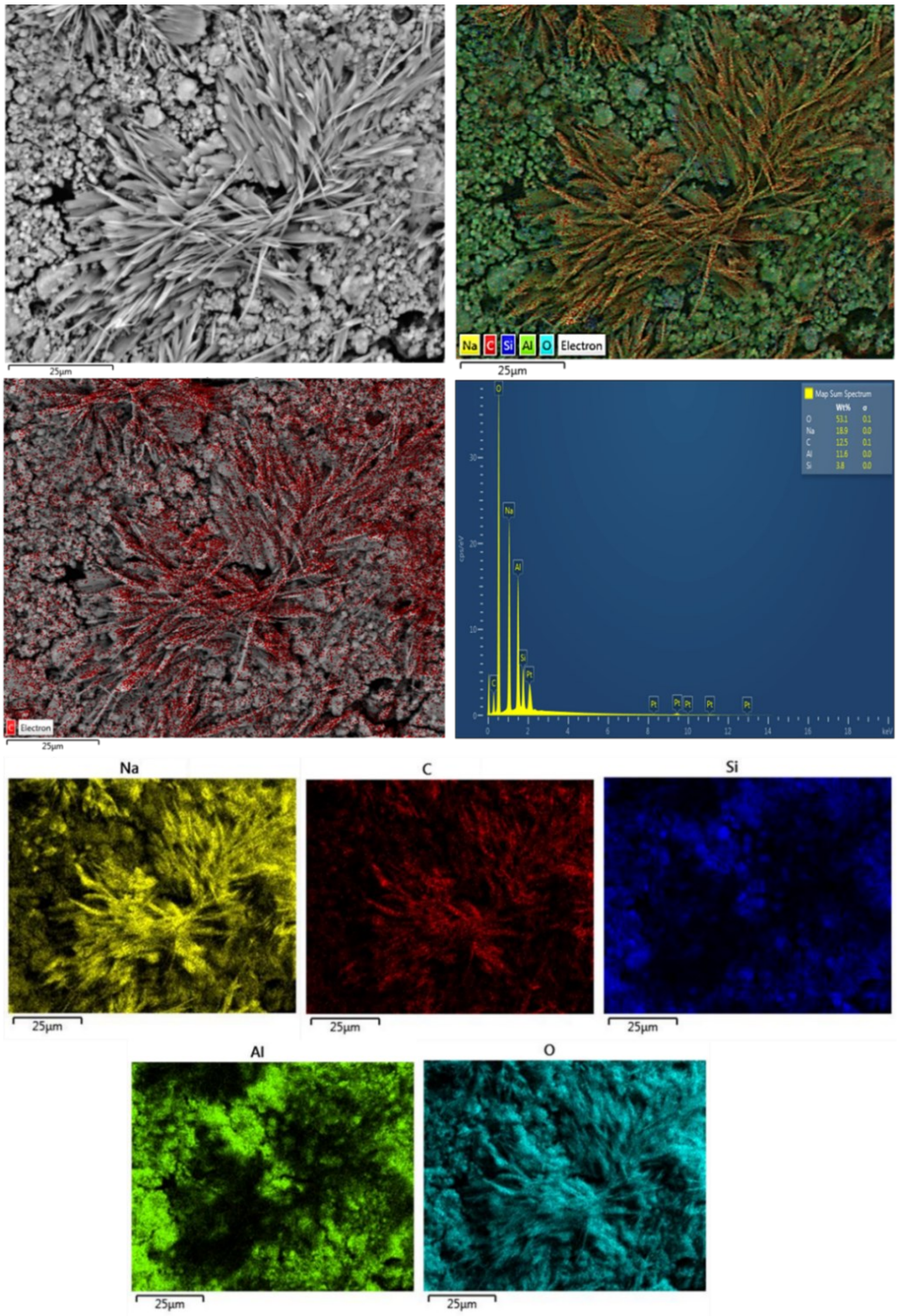

Fig. S9. SEM-EDX elemental mapping of the surface of CNCs-Y seed gel composite.

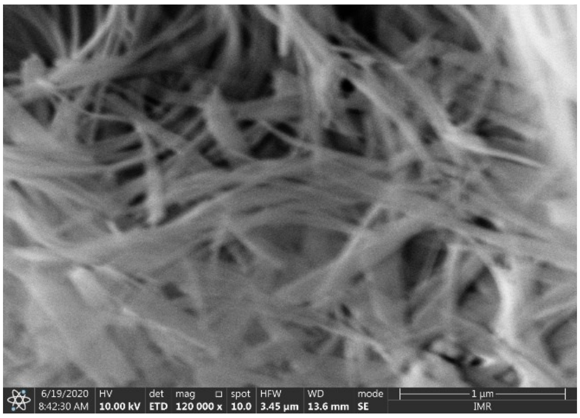

Fig. S10. (a)–(c) SEM micrographs of the as-synthesised CNTs-Y.

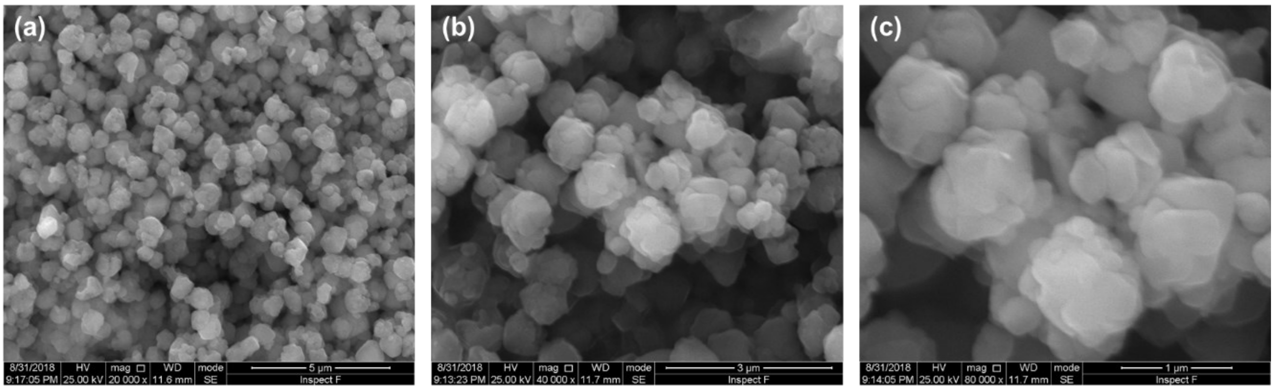

Fig. S11. (a)–(c) SEM micrographs of the as-synthesised CNTs-Y.

Solid-state nuclear magnetic resonance (NMR)

Solid-state NMR spectra were recorded on an Agilent 600 DD2 spectrometer operating at a Larmor frequency of 600 MHz for 1H. ^{29}Si magic angle spinning (MAS) NMR spectra were recorded at 119.15 MHz (with the proton decoupling (TPPM) during acquisition) using a 3.6 µs pulse with a 30 s recycle delay and 1024 scans (tetramethylsilane as the reference).

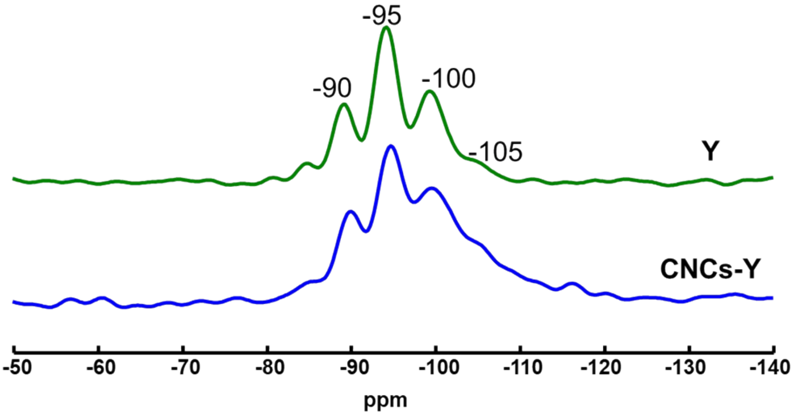

Fig. S12. ^{29}Si MAS NMR spectra of Y and CNCs-Y.

Catalytic results

Exemplar GC Chromatographs of the Pulse Method for Catalyst Evaluation

The 1st Injection

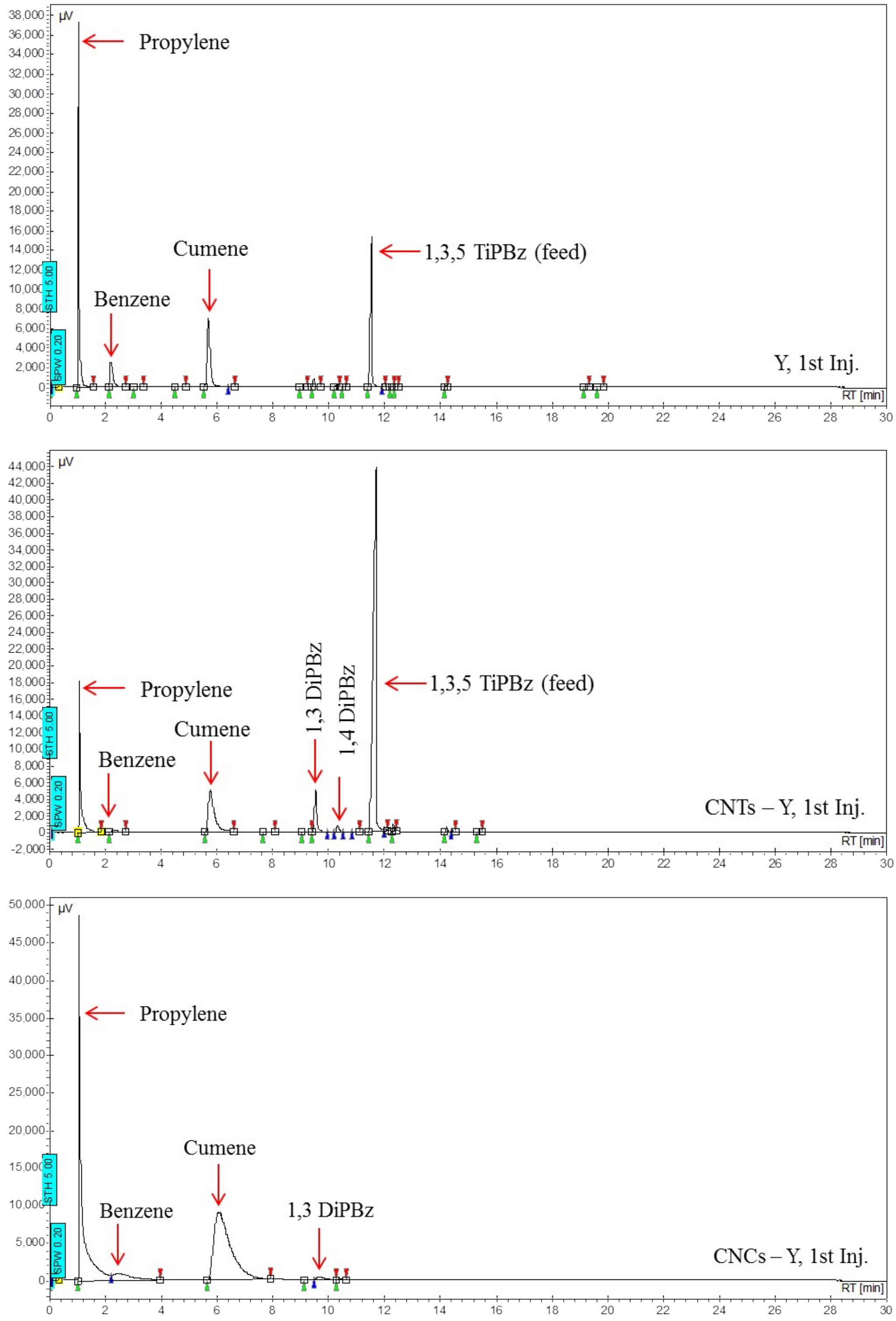

Fig. S13. GC chromatograph analysis of the 1st injection in the catalytic tests.

The 17th injection

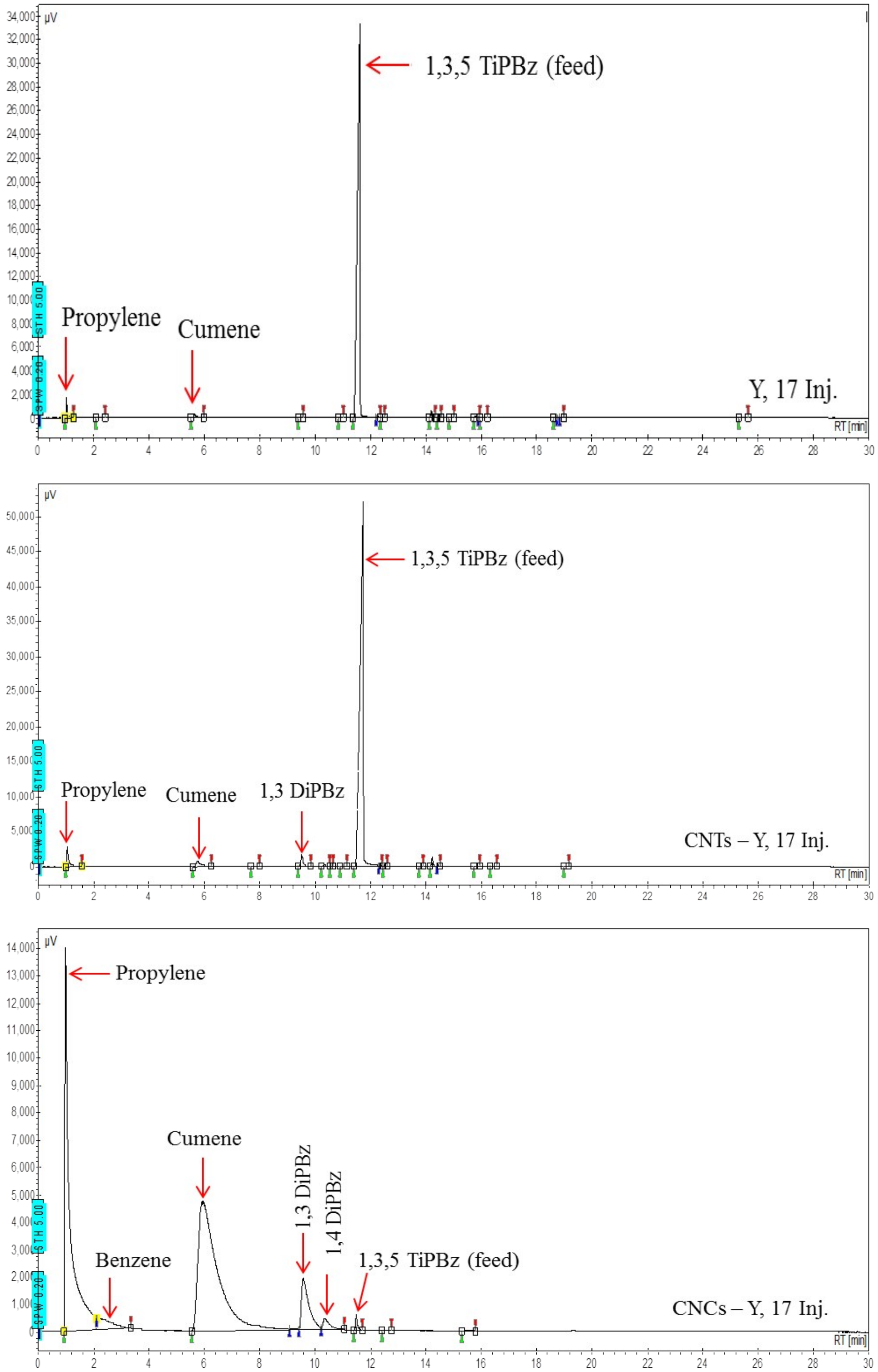

Fig. S14. GC chromatograph analysis of the 17th injection in the catalytic tests.

Selectivity and Yield

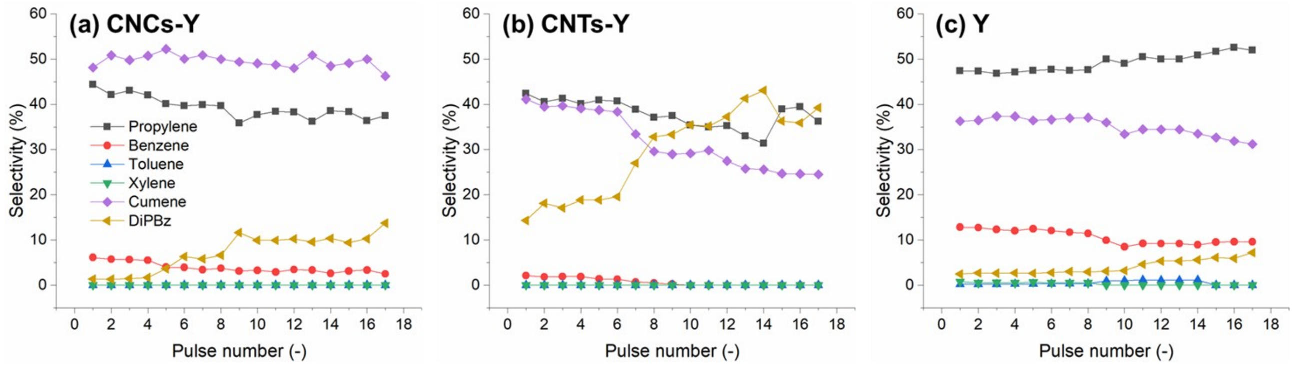

Fig. S15. Product selectivity of catalytic TiPBz cracking over (a) CNCs-Y, (b) CNTs-Y, (c) Y.

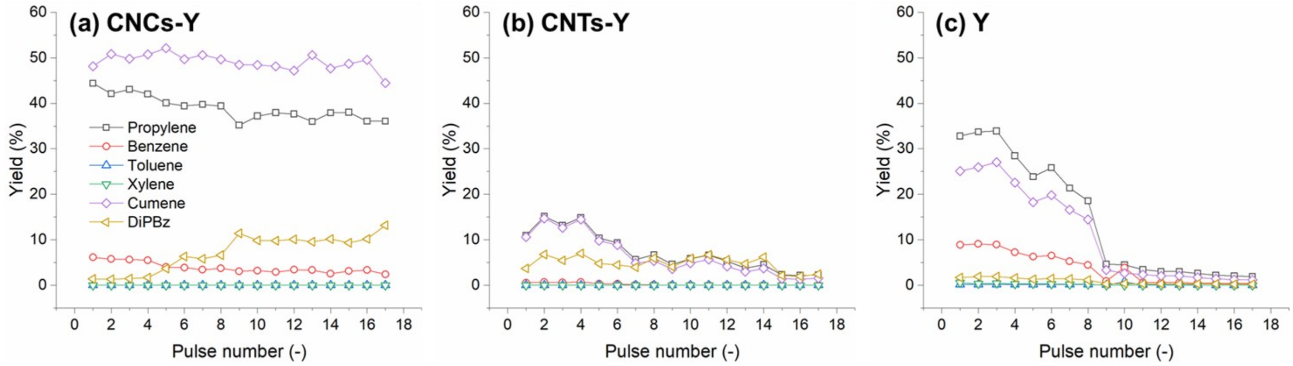

Fig. S16. Product yield of catalytic TiPBz cracking over (a) CNCs-Y, (b) CNTs-Y, (c) Y.

NH_3-TPD analysis of Y, CNTs-Y and CNCs-Y Zeolites

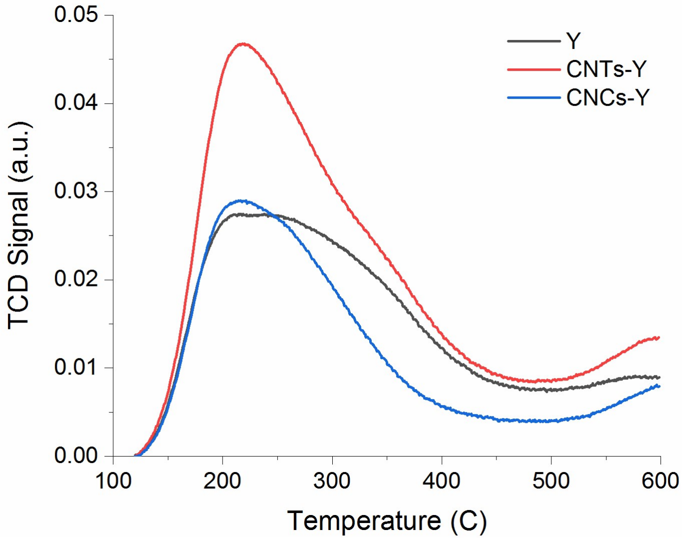

Fig. S17. NH_3-TPD profiles of Y, CNTs-Y and CNCs-Y zeolites (after ion exchange).

Comparison of Mesoporous Properties of Y Zeolites by the ‘Bottom-up’ Methods

Table S2. Comparison the specific external surface area (S_{external}) and mesopore volume (V_{meso}) of mesoporous Y zeolites prepared by ‘bottom-up’ methods using soft/hard templates.

Synthesis strategy	Templates	S_{external} [m^2 g^{-1}]	V_{meso} [cm^3 g^{-1}]	Ref.
Hard templating	Multiwall CNTs	69	0.09	this work
	Carbon aerogels (monolithic form)	-	1.37	8
	Three-dimensionally ordered mesoporous (3Dom) carbon	208	0.39	9
	CNCs	347	0.52	this work
Soft templating	CTAB, [C$_{16}$MIm]CL, [C$_{16}$MPy]CL	-	0.31–0.39	10
	Pluronic P123 ($PEO_{20}PPO_{70}PEO_{20}$) – block copolymer	-	0.12–0.18	11
	Pluronic F127 (PEO_{106}-PPO_{70}-PEO_{106}) – block copolymer	-	0.2	12
	TPOACl – bifunctional ammonium salt	75–144	0.18–0.29	13
	TPOAB	137	0.2	
	TPHAC – amphiphilic organosilane surfactant	-	0.27	14
	TPHAC – functionalised with hydrophilic hydroxyl groups	179	0.26	15
	Trimethoxysilylpropyl imidazolium chloride – bifunctional ionic liquid	90	-	16

References

1. M. A. Atieh, O. Y. Bakather, B. Al-Tawbini, A. A. Bukhari, F. A. Abuilaiwi and M. B. Fettouhi, *Bioinorganic chemistry and applications*, 2010, DOI: 10.1155/2010/603978, 603978.
2. M. F. Alkhatib, M. E. S. Mirghani, I. Y. Qudsieh and I. A. Husain, *Journal of Applied Sciences*, 2010, **10**, 2705-2708.
3. Anuj Kumar, Yuvraj Singh Negi, Veena Choudhary and N. K. Bhardwaj, *Journal of Materials Physics and Chemistry*, 2014, **2**, 1-8.
4. C. Zhang, M. R. Salick, T. M. Cordie, T. Ellingham, Y. Dan and L. S. Turng, *Materials science & engineering. C, Materials for biological applications*, 2015, **49**, 463-471.
5. P. Li, T. Ding, L. Liu and G. Xiong, *Materials Characterization*, 2013, **86**, 221-231.
6. M. Tavasoli, H. Kazemian, S. Sadjadi and M. Tamizifar, *Clays and Clay Minerals*, 2014, **62**, 508-518.
7. P. K. Jatuporn Wittayakun, Sanchai Prayoonpokarach, *25*, 2008, **4**, 861-864.
8. H. K. Yousheng Tao, Katsumi Kaneko, *J. Phys. Chem. B*, 2003, **107**, 10974-10976
9. H. Chen, J. Wydra, X. Zhang, P. S. Lee, Z. Wang, W. Fan and M. Tsapatsis, *Journal of the American Chemical Society*, 2011, **133**, 12390-12393.
10. A. Sachse, C. Wuttke, U. Díaz and M. O. de Souza, *Microporous and Mesoporous Materials*, 2015, **217**, 81-86.
11. J. Zhao, G. Wang, L. Qin, H. Li, Y. Chen and B. Liu, *Catalysis Communications*, 2016, **73**, 98-102.
12. J. Zhao, Y. Yin, Y. Li, W. Chen and B. Liu, *Chemical Engineering Journal*, 2016, **284**, 405-411.
13. J. Jin, C. Peng, J. Wang, H. Liu, X. Gao, H. Liu and C. Xu, *Industrial & Engineering Chemistry Research*, 2014, **53**, 3406-3411.
14. M. Qamar, I. Baig, A. M. Azad, M. I. Ahmed and M. Qamaruddin, *Chemical Engineering Journal*, 2016, **290**, 282-289.
15. Z. Wang, H. H. Liu, Q. T. Meng, J. S. Jin, C. Y. Xu, X. T. Mi, X. H. Gao and H. T. Liu, *RSC Advances*, 2017, **7**, 9605-9609.
16. X. Fu, X. Sheng, Y. Zhou, Z. Fu, S. Zhao, X. Bu and C. Zhang, *RSC Advances*, 2016, **6**, 50630-50639.